CrystEngComm

Accepted Manuscript

ROYAL SOCIETY OF CHEMISTRY

www.rsc.org/crystengcomm

Cite this: DOI: 10.1039/c0xx00000x

www.rsc.org/xxxxxx

ARTICLE TYPE

Raman spectroscopy and density functional theory analyses of the melt structure in $Li_2B_4O_7$ crystal growth system

Songming Wan,*[a] Xiaolu Tang,[a] Yulong Sun,[a] Guochun Zhang,[b] Jinglin You[c] and Peizhen Fu[b]

Received (in XXX, XXX) Xth XXXXXXXXX 20XX, Accepted Xth XXXXXXXXX 20XX

DOI: 10.1039/b000000x

Melt structure, a fundamental and challenging subject for borate crystal growth, has not been solved for many years. In this paper, a new method has been employed to study $Li_2B_4O_7$ melt structure. High-temperature Raman spectroscopy has been used to investigate the structural evolvement from $Li_2B_4O_7$ crystal to $Li_2B_4O_7$ melt. Based on the investigation, a model was proposed to describe the $Li_2B_4O_7$ melt. The melt is built up of polymer-like boron−oxygen chains; the minimal repeated unit is the $B_4O_6Ø_2^{2-}$ (Ø = bridging oxygen) group which is formed by a $B_3O_4Ø_2^-$ six-membered ring and a $BOØ_2^-$ triangle linked by a bridging oxygen atom. DFT calculations have verified the melt structure and provided accurate assignments for the vibrational bands present in $Li_2B_4O_7$ melt Raman spectrum.

1. Introduction

Lithium tetraborate ($Li_2B_4O_7$) single crystal has attracted great attention for use in many fields inculding surface acoustic wave,[1] bulk acoustic wave,[2] non-linear optics[3] and neutron detection.[4] The crystal is usually grown from $Li_2B_4O_7$ melt by Czochralski[5] or Bridgman method.[6] High viscosity of the $Li_2B_4O_7$ melt, like other borate melts, is not beneficial to the successful preparation of large and high-quality $Li_2B_4O_7$ single crystals. For example, as a result of the high viscosity, bubbles and voids were often found heavily concentrated at the central part of the crystal boules.[5, 6]

Melt structure is an intrinsic factor governing a variety of melt macro-properties, including viscosity, density and surface tension.[7] Deep understanding on the $Li_2B_4O_7$ melt structure in $Li_2B_4O_7$ crystal growth system can help us to better interpret the crystal growth phenomena and then to improve crystal quality. On the other hand, it is known that $Li_2B_4O_7$ crystal structure is transformed from the melt structure.[8] Therefore, some important information of $Li_2B_4O_7$ crystal growth process on molecular scale can be obtained based on the study of the $Li_2B_4O_7$ melt structure. However, despite the imporatance of borate melt structure, a detailed study on it has not been conducted up to now. In the past, a borate melt structure was usually extrapolated from the glass structure of the same stoichiometry. Actually, a glass structure is the super-cooled melt structure frozen at the glass transition temperature rather than the true high-temperature melt structure.[9]

Accurate investigation of a melt structure requires high-temperature *in-situ* experimental techniques. In comparison to other experimental techniques, Raman spectroscopy is regarded as an effective and convenient *in-situ* method for the study of melt structures.[8, 10] However, the conversion of the vibrational peaks seen in a Raman spectrum into the structural information remains difficult.[11]

Recently, density functional theory (DFT) method has been used to predict and interpret Raman spectra for a wide range of materials, including crystals, polymers and molecules.[12] It provides a possibility to study a melt structure and simulate its Raman spectrum. In this paper, we proposed a new and general method, which combines high-temperature Raman spectroscopy with DFT calculation, to study the melt structure in $Li_2B_4O_7$ crystal growth system.

2. Experimental

A homemade micro-furnace used in this work was described elsewhere.[8] A $Li_2B_4O_7$ crystal slice with a size of 10 × 5 × 1 mm^3 was placed into a platinum boat, and then into the micro-furnace with the boat. The micro-furnace provided a horizontal temperature gradient in the boat. The crystal and melt Raman spectra were recorded with a Jobin Yvon LabRaman HR800 Raman spectrometer in a back scattering configuration. The Raman scattering light was collected by a confocal lens system, and then recorded by an intensive charge couple device (ICCD). The excitation source was the 355 nm line of a Q-switch pulsed THG-Nd:YAG laser with an average output of 0.9 W. The diameter of the laser beam was less than 2 μm. The instrumental resolution was ± 0.1 cm^{-1} with a repeatability of ± 1 cm^{-1}. The spectral acquisition, under an accumulated mode, was preformed for 50 s integration time (5 scans, scan time 10 s each). The spectral collecting range was 70−2000 cm^{-1}.

3. Computational Details

All calculations were carried out using a plane wave basis-set and norm-conserving pseudopotentials as implemented in CASTEP (Cambridge Sequential Total Energy Package) code.[13] Exchange and correlation energies were approximated using the Perfew−Burke−Ernzerh functional of generalized gradient approximation (GGA-PBE).[14] The plane-wave energy cutoff and

the convergence criterion of self-consistent field (SCF) were 950 eV and 10^{-6} eV/atom, respectively. The Brillouin zone integrations were done over a 2 × 2 × 2 Monkhorst−Pack grid for the crystal and over a 2 × 4 × 2 Monkhorst−Pack grid for the melt. The experimentally determined $Li_2B_4O_7$ crystal structure[15] and the proposed $Li_2B_4O_7$ melt structure were used as the initial structures for structural optimization and Raman spectrum calculation.[15] All calculated Raman intensities were corrected by Bose-Einstein factors with the experimental temperatures (300 K for the crystal and 1200 K for the melt) and the excitation source wavelength (355 nm). The Raman peaks were broadened with Gaussian shape functions using the SWizard program.[16]

4. Results and Discussion

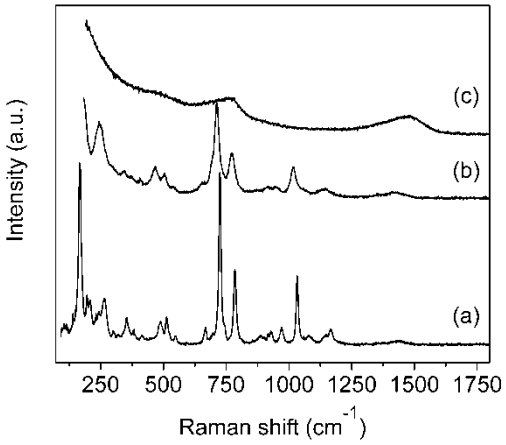

Fig. 1 Raman spectra of $Li_2B_4O_7$ crystal and melt. (a) crystal Raman spectrum at 30 °C; (b) crystal Raman spectrum at 500 °C; (c) melt Raman spectrum near the melting point.

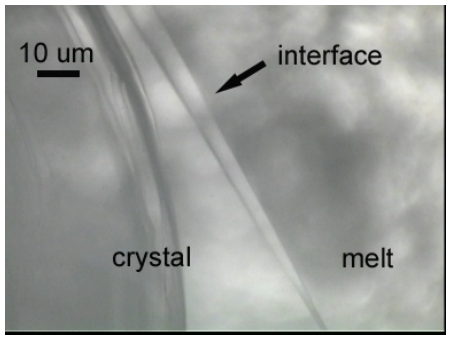

Fig. 2 A typical $Li_2B_4O_7$ crystal−melt interface.

Crystal Raman spectra were recorded at different temperatures. The cases at 30 °C and 500 °C are shown in Fig. 1a and 1b, respectively. With an increase of temperature, all Raman peaks red-shifted and broadened in different degrees. When the hot end was heated over the melting point, the crystal began to melt. After that, the temperature was slowly decreased until a steady crystal–melt interface presented (see Fig. 2). The melt Raman spectra were recorded near the interface to ensure the measuring temperature close to the crystal growth temperature. A typical melt Raman spectrum is shown in Fig. 1c. Comparing with the crystal Raman spectra, we found that: (1) the intensive crystal peaks located around 720 cm^{-1} and in the region of 900−1200 cm^{-1} disappeared in the melt Raman spectrum; (2) The Raman peaks in the high frequency region (1300−1500 cm^{-1}) anomalously blue-shifted and increased in intensity when the crystal melted.

Our aim is to obtain the $Li_2B_4O_7$ melt structure in $Li_2B_4O_7$ crystal growth system. $Li_2B_4O_7$ crystal structure has been determined by X-ray single crystal diffraction method. If the structural evolvement details from $Li_2B_4O_7$ crystal to melt are disclosed, the melt structure will be derived. In this work, the evolvement details are reflected by the Raman spectrum changes during the $Li_2B_4O_7$ crystal melting process.

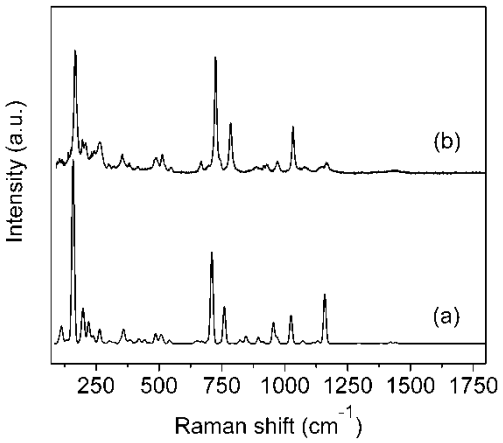

Fig. 3 (a) Calculated and (b) experimental Raman spectra of $Li_2B_4O_7$ crystal.

In order to disclose the structural origins of the spectral changes, some important crystal Raman peaks should be assigned. The $Li_2B_4O_7$ crystal structure solely consists of $B_4O_5Ø_4^{2-}$ groups (Ø = bridging oxygen, as shown in Fig. S1) except for Li^+ ions. Structural complexity of $B_4O_5Ø_4^{2-}$ group makes it very difficult to give an exact assignment for each crystal Raman peak. Generally, the Raman peaks were approximately assigned to the vibrations of $BØ_4^-$ tetrahedrons and of $BØ_3$ triangles (two basic structural units constituting the $B_4O_5Ø_4^{2-}$ group) although the two units are not independent.[17] In this paper, we used the DFT method implemented in CASTEP code to calculate the $Li_2B_4O_7$ crystal Raman spectrum for the first time and intended to give clearer assignments to some important vibrational peaks. The calculated results give 153 optical modes ($18A_1 + 19A_2 + 19B_1 + 19B_2 + 39E$), among these, 134 modes ($18A_1 + 19B_1 + 19B_2 + 39E$) are Raman active (see the supporting information, Table S1). These results are in agreement with group-theory analysis.[17] The calculated Raman spectrum is shown in Fig. 3, along with the experimental spectrum. All calculated frequencies coincide well with the experimental within an acceptable error (20 cm^{-1}). The relative intensities of the calculated peaks are also consistent with the experimental results except some weak experimental peaks, such as 259 cm^{-1}, 960 cm^{-1} and 1150 cm^{-1} peaks. The theoretical agreement with experiment confirms the validity of our calculation method.

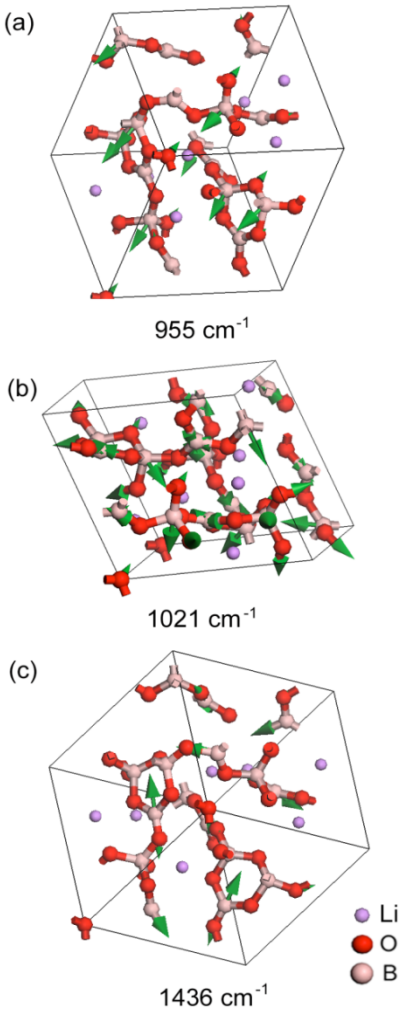

Fig. 4 Atomic displacements of three important crystal vibrational peaks.

According to the calculated results, some key Raman peaks were assigned. The intensive peaks located in the range of 900−1200 cm^{-1} mainly arise from the asymmetrical vibrations of the $BØ_4^-$ units. The atomic displacements of 955 cm^{-1} and 1021 cm^{-1} peaks are shown in Fig. 4. These peaks disappeared in the melt spectrum, suggesting that the $BØ_4^-$ units converted into other boron−oxygen units during the melting process, such as $BOØ_2^-$ (a boron–oxygen triangle consisting of two bridging oxygen atoms and one non-bridging oxygen atom) caused by the break of B_4−Ø bonds (the B−Ø bond of a $BØ_4^-$ tetrahedron), as found in many other borate melts.[18] The weakness of the B_4−Ø bonds is also supported by the crystal habit. For example, Pan et al. found that $Li_2B_4O_7$ crystal easily cracks along the {112} faces which are connected by the B_4−Ø bonds (see the supporting information, Fig. S1).[19]

The vibrational bands in the 600−850 cm^{-1} region are related to the breathing vibrations of boron−oxygen six-membered rings.[18, 20] During the melting process, the crystal 720 cm^{-1} peak disappeared and 770 cm^{-1} peak remained, indicating boron−oxygen six-membered rings still remained in the melt although their structures were different from those in $Li_2B_4O_7$ crystal structure.

The high-frequency crystal peaks located around 1435 cm^{-1} are related to the stretching vibrations of the extra-ring B_3−Ø bonds (the B−Ø bond of a $BØ_3$ triangle), as shown in Fig. 4c. The peaks anomalously blue-shifted to 1480 cm^{-1} in the melt Raman spectrum, indicating new boron−oxygen structural units formed in the melt. Generally, strong Raman peaks located around 1500 cm^{-1} are attributed to the stretching vibrations of extra-ring B_3−O bonds,[20] which implies that the extra-ring B_3−Ø bonds in the crystal structure changed to the extra-ring B_3−O bonds when the crystal melted.

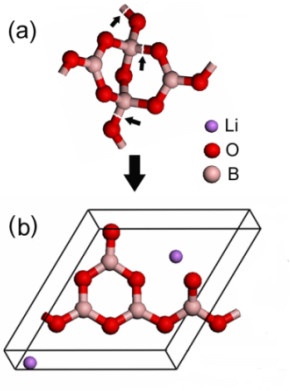

Fig. 5 Structural evolvement of $Li_2B_4O_7$ crystal to $Li_2B_4O_7$ melt. (a) basic boron−oxygen structural group in $Li_2B_4O_7$ crystal; (b) basic structural group in $Li_2B_4O_7$ melt.

By investigating the structural evolvement in the melting process, we found that the B_4−Ø bonds in the $Li_2B_4O_7$ crystal structure were broken. As a result, new boron−oxygen six-membered rings with extra-ring non-bridging oxygen atoms appeared in the melt. In term of the structural evolvement, we deduced the $Li_2B_4O_7$ melt structure. The melt is build up of polymer-like boron−oxygen chains; the minimal repeated unit of the chain is the $B_4O_6Ø_2^{2-}$ group which is formed by a $B_3O_4Ø_2^-$ six-membered ring and a $BOØ_2^-$ triangle linked by a bridging oxygen atom, as shown in Fig. 5b.

The $Li_2B_4O_7$ melt structure was verified by DFT calculation. In general, DFT calculations are performed in three-dimensional periodic systems; however, the $Li_2B_4O_7$ melt is non-periodic. In order to simulate the melt structure, a super-cell method was used.[21] One minimal repeated unit ($B_4O_6Ø_2^{2-}$ group) was placed into a unit cell; two Li^+ ions were put into the same unit cell to balance the charge of the boron−oxygen group (see Fig. 5b). Considering the strong electrostatic interactions between the chains and Li^+ ions, we did not limit the unit cell parameters and the atomic positions during the DFT geometry optimization.[22] After the most stable structure was achieved, its Raman spectrum was calculated at the same level of theory for the $Li_2B_4O_7$ crystal Raman spectrum calculation.

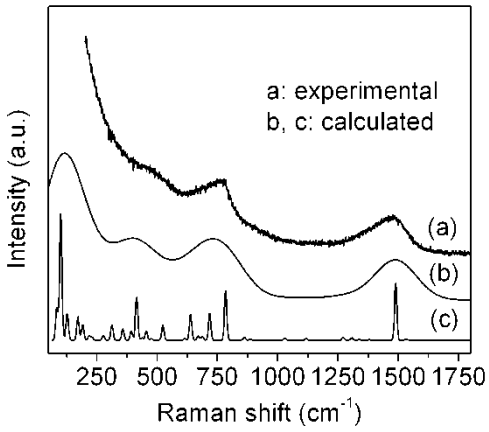

Fig. 6 Experimental and calculated Raman spectra of $Li_2B_4O_7$ melt. (a) experimental Raman spectrum; (b) calculated Raman spectrum broadened by Gaussian line shape function with a FWHM of 200 cm^{-1}; (c) calculated Raman spectrum broadened by Gaussian line shape function with a FWHM of 10 cm^{-1}.

The optimized melt structural unit (the minimal repeated unit) is shown in Fig. 5b. The calculated B–O bond lengths and O–B–O angles are all in agreement with the reported values (see the supporting information, Fig. S2 and Table S2). The calculated results give 36 modes (36A) of Raman active, which is in agreement with that of group-theory analysis (see the supporting information, Table S3). The calculated $Li_2B_4O_7$ melt Raman spectra, together with the experimental spectrum, are shown in Fig. 6. The temperature dependence (thermal broadening) of the Raman peak shape was simulated by a Gaussian line shape function with a FWHM (full width at half maximum) of 200 cm^{-1}.[16] The superposition of these Gaussian profiles is shown in Fig. 6b. All of the calculated frequencies and intensity are consistent with the experimental results, which confirms our inference that the $Li_2B_4O_7$ melt is built up of the $B_4O_6Ø_2^{2-}$ chains.

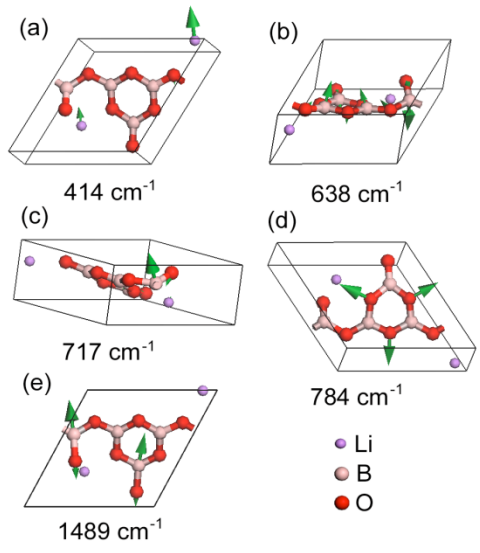

Fig. 7 Atomic displacements of five strong peaks in calculated $Li_2B_4O_7$ melt Raman spectrum.

The calculated results further provide accurate assignments for three main vibrational bands present in the melt Raman spectrum (see Fig. 6). (1) The Raman band in the range of 250−500 cm^{-1} is related to the motions of the Li^+ ions. (2) The Raman band in the range of 600−800 cm^{-1} includes three strong peaks, respectively located at 638 cm^{-1}, 717 cm^{-1} and 784 cm^{-1}. The 638 cm^{-1} peak and the 717 cm^{-1} peak are mainly attributed to the out-plane bending vibrations of the boron–oxygen triangle; the 784 cm^{-1} peak is related to the breathing vibration of the boron–oxygen six-membered ring. (3) The high-frequency band from 1300 cm^{-1} to 1600 cm^{-1} primarily arises from the stretching vibration of the extra-ring B_3−O bond. The atomic displacements of the five strong peaks are shown in Fig. 7.

5. Conclusions

In order to obtain the melt structure in $Li_2B_4O_7$ crystal growth system, Raman spectroscopy and DFT method were used to investigate the structural evolvement from $Li_2B_4O_7$ crystal to melt. During the crystal melting process, the B_4−Ø bonds in the crystal structure were broken. As a result, new boron−oxygen six-membered rings with extra-ring non-bridging oxygen atoms appeared in the melt. According to the structural evolvement, we proposed a structural model to describe the melt. The melt is built up of polymer-like chains; their minimal repeated unit is the $B_4O_6Ø_2^{2-}$ group which is formed by a $B_3O_4Ø_2^-$ six-membered ring and a $BOØ_2^-$ triangle linked by a bridging oxygen atom.

The Raman spectrum of the $Li_2B_4O_7$ melt was calculated by DFT method. The calculated Raman spectrum is consistent with the experimental. The Raman band in the range of 250−500 cm^{-1} is related to the motions of the Li^+ ions; the Raman band in the range of 600−800 cm^{-1} is mainly attributed to the out-plane bending vibrations of the boron–oxygen triangle and the breathing vibration of the six-membered ring; the Raman band in the range of 1300−1600 cm^{-1} primarily arises from the stretching vibrations of the extra-ring B_3−O bond.

We believe that the method provided in this paper can be extended to investigation of other borate melt structures and help us deeply understand the macro-properties of borate melts and the micro-process in borate crystal growth.

Acknowledgment

This work is financially supported by the National Natural Science Foundation of China (Grant No. 50932005 and 51372246). The authors are also grateful to Prof. Liang Shi and Jian Chen for their helpful discussion.

Notes and references

[a] *Anhui Key Laboratory for Photonic Devices and Materials, Anhui Institute of Optics and Fine Mechanics, Chinese Academy of Sciences, Hefei 230031, China.*
E-mail: smwan@aiofm.ac.cn; Fax: +86 0551 65591054; Tel: +86 0551 65591054;
[b] *Technical Institute of Physics and Chemistry, Chinese Academy of Sciences, Beijing 100190, P. R. China*
[c] *School of Material Science and Engineer, Shanghai University, Shanghai 200072, China.*
† Electronic Supplementary Information (ESI) available: Calculated optical modes of $Li_2B_4O_7$ crystal and melt and their frequencies, Atomic configuration of the (112) face in $Li_2B_4O_7$ crystal structure and the optimized melt structure. See DOI: 10.1039/b000000x/

1 R. W. Whatmore, N. M. Shorrocks, C. Ohara, F. W. Ainger and I. M. Yong, *Electron. Lett*., 1981, **17**, 11−12.

2 K. S. Aleksandrov, P. P. Turchin, B. P. Sorokin, A. A. Karpovich and V. A. Nefedov, IEEE/EIA International Frequency Control Symposium and Exhibition, Kansas city, 2000.

3 R. Komatsu, T. Sugawara, K. Sassa, N. Sarukura, Z. Liu, S. Izumida, Y. Segawa, S. Uda, T. Fukuda and K. Yamanouchi, *Appl. Phys. Lett*., 1997, **70**, 3492−3494.

4 T. Nakamura, M. Katagiri, K. Soyama, M. Ukibe, T. Ikeuchi and M. Ohkubo, *Nucl. Instrum. Methods Phys. Res., Sect. A,* 2004, **529**, 402−404.

5 S. Kar and K. S. Bartwal, *Cryst. Growth Des*., 2007, **7**, 2522−2525.

6 N. Tsutsui, Y. Ino, K. Imai, N. Senguttuvan and M. Ishii, *J. Cryst. Growth* 2001, **229**, 283−288; J. Y. Xue, S. J. Fan and B. L. Lu, *J. Cryst. Growth,* 2004, **264**, 260−265.

7 O. Majerus, L. Cormier, G. Calas and B. Beuneu, *J. Phys. Chem. B* 2003, **107**, 13044−13050; J. R. Allwardt, J. F. Stebbins, H. Terasaki, L. S. Du, D. J. Frost, A. C. Withers, M. M. Hirschmann, A. Suzuki and E. Ohtani, *Am. Mineral.,* 2007, **92**, 1093−1104.

8 S. M. Wan, X. Zhang, S. J. Zhao, Q. L. Zhang, J. L. You, L. Lu, P. Z. Fu, Y. C. Wu and S. T. Yin, *Cryst. Growth Des.,* 2008, **8**, 412−414; D. Wang, S. M. Wan, S. T. Yin, Q. L. Zhang, J. L. You, G. C. Zhang and P. Z. Fu, *CrystEngComm,* 2011, **13**, 5239−5242; X. S. Lv, Y. L. Sun, X. L. Tang, S. M. Wan, Q. L. Zhang, J. L. You and S. T. Yin, *J. Cryst. Growth,* 2013, **371**, 107−111.

9 M. Orrit, *Angew. Chem. Int. Ed*., 2012, **52**, 163−166; H. Krebs, *Angew. Chem. Int. Ed.,* 1966, **5**, 544−554.

10 D. P. Shoemaker, D. Y. Chung, J. F. Mitchell, T. H. Bray, L. Soderholm, P. J. Chupas and M. G. Kanatzidis, *J. Am. Chem. Soc.,* 2012, **134**, 9456−9463.

11 B. N. Meera and J. Ramakrishna, *J. Non-Cryst. Solids,* 1993, **159**, 1−21; R. J. Heaton and P. A. Madden, *Mol. Phys*., 2008, **106**, 1703−1719.

12 V. Milman, K. Refson, S. J. Clark, C. J. Pickard, J. R. Yates, S. P. Gao, P. J. Hasnip, M. I. J. Probert, A. Perlov and M. D. Segall, *J. Mol. Struct.: THEOCHEM,* 2010, **954**, 22−35; V. Milman, A. Perlov, K. Refson, S. J. Clark, J. Gavartin and B. Winkler, *J. Phys.: Condens. Mat.,* 2009, **21**, 485404.

13 M. D. Segall, Philip J. D. Lindan, M. J. Probert, C. J. Pickard, P. J. Hasnip, S. J. Clark and M. C. Payne, *J. Phys.: Condens. Mat.,* 2002, **14**, 2717−2744.

14 J. P. Perdew, K. Burke and M. Ernzerhof, *Phys. Rev. Lett*., 1996, **77**, 3865−3868.

15 S. Natalis, B. Rimman, S. Jurii, F. Stanislav and Y. Olga, *J. Alloy Compd.,* 2007, **428**, 290−296.

16 S. I. Gorelsky and A. B. P. Lever, *J. Organomet. Chem.,* 2001, **635**, 187−196.

17 G. L. Paul and W. Taylor, *J. Phys. C: Solid State Phys.,* 1982, **15**, 1753−1764; A. E. Elalaoui, A. Maillard and M. D. Fontana, *J. Phys.: Condens. Mat.,* 2005, **17**, 7441−7454.

18 O. Majérus, L. Cormier, G. Calas and B. Beuneu, *Phys. Rev. B,* 2003, **67**, 024210; T. Yano, N. Kunimine, S. Shibata and M. Yamane, *J. Non-Cryst. Solids,* 2003, **321**, 137−168.

19 Z. L. Pan, J. C. Yang, Z. H. Shen, X. H. Yue, G. S. Shen and J. L. Li, *J. Inorg. Mater.,* 1994, **9**, 209−213.

20 E. I. Kamitsos, M. A. Karakassides and G. D. Chryssikos, *Phys. Chem. Glasses,* 1989, **30**, 229−234.

21 G. Zheng, S. J. Clark, S. Brand and R. A. Abram, *Phys. Rev. B,* 2006, **74**, 165210; T. T. Lin, X. Y. Liu and C. B. He, *J. Phys. Chem. B,* 2012, **116**, 1524−1535.

22 Y. L. Sun, S. M. Wan, X. S. Lv, X. L. Tang, J. L. You and S. T. Yin, *CrystEngComm,* 2013, **15**, 995−1000.

Table of Contents Entry

Raman spectroscopy and density functional theory analyses of the melt structure in $Li_2B_4O_7$ crystal growth system

Songming Wan, Xiaolu Tang, Yulong Sun, Guochun Zhang, Jinglin You and Peizhen Fu

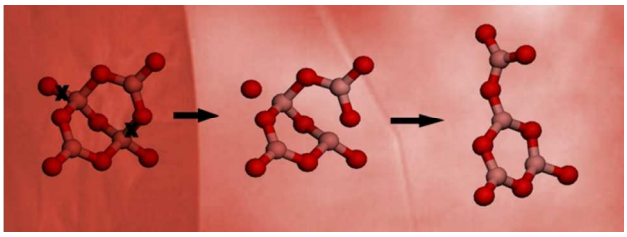

Raman spectroscopy and density functional theory method were applied to study $Li_2B_4O_7$ melt structure, a new boron–oxygen chain structure was found for the first time.